

# Empennage Noise Shielding Benefits for an Open Rotor Transport

Jeffrey J. Berton\*

NASA Glenn Research Center, Cleveland, Ohio 44135

NASA sets aggressive, strategic, civil aircraft performance and environmental goals and develops ambitious technology roadmaps to guide its research efforts. NASA has adopted a phased approach for community noise reduction of civil aircraft. While the goal of the near-term first phase focuses primarily on source noise reduction, the goal of the second phase relies heavily on presumed architecture changes of future aircraft. The departure from conventional airplane configurations to designs that incorporate some type of propulsion noise shielding is anticipated to provide an additional 10 cumulative EPNdB of noise reduction. One candidate propulsion system for these advanced aircraft is the open rotor engine. In some planned applications, twin open rotor propulsors are located on the aft fuselage, with the vehicle's empennage shielding some of their acoustic signature from observers on the ground. This study focuses on predicting the noise certification benefits of a notional open rotor aircraft with tail structures shielding a portion of the rotor noise. The measured noise of an open rotor test article – collected with and without an acoustic barrier wall – is the basis of the prediction. The results are used to help validate NASA's reliance on acoustic shielding to achieve the second phase of its community noise reduction goals. The noise measurements are also compared to a popular empirical diffraction correlation often used at NASA to predict acoustic shielding.

## Nomenclature

$a_i$	=	calibration constants introduced in Maekawa diffraction model
$c$	=	speed of sound, ft/s
$f$	=	frequency, Hz
$IL$	=	insertion loss (barrier-shielding attenuation), dB
$M_{Flight}$	=	flight Mach number
$M_{Tunnel}$	=	wind tunnel Mach number
$N_F$	=	Fresnel number, $2f\Delta/c$
$\Delta$	=	characteristic length of Fresnel number
$\theta_E$	=	emission yaw angle
$\theta_G$	=	geometric yaw angle

## I. Introduction

Rising, unstable fuel prices are spurring research into advanced, energy-efficient propulsion concepts for transport aircraft. As a result, rekindled attention is being given to open rotor propulsion systems. Once hailed as an innovative response to the sharp increases in aviation fuel cost beginning in 1973, interest in open rotors waned in the face of falling oil prices starting in 1986. Current energy concerns are reviving development efforts into open rotor propulsors (alternately known as advanced turboprops, propfans, or unducted fans).

Counter-rotating open rotor propulsion systems – with highly-swept, contoured, wide-chord rotor blades – combine the fuel efficiency of traditional turboprops with the high cruising airspeed of turbofan engines. Without inlet and bypass exhaust ducts, however, an unfortunate disadvantage of the open rotor relative to ducted turbofans may be higher community noise. Although promising low-noise rotor designs exist, and although any eventual open rotor aircraft will necessarily have to meet all noise certification requirements, it is likely that open rotor propulsion

---

\* Aerospace Engineer, Multidisciplinary Design, Analysis and Optimization Branch, MS 5-11, senior member AIAA.

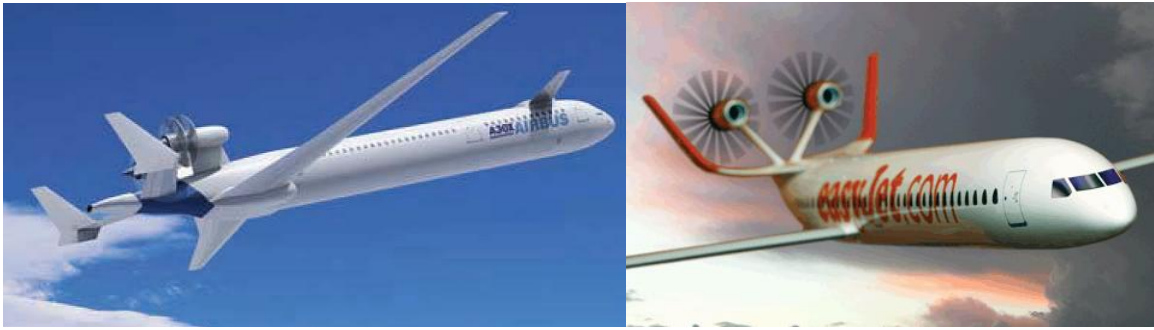


**Figure 1. Proposed Airbus A30X and easyJet ecoJet open rotor airplane candidates having potential empennage shielding benefits (Refs. 6, 7).**

systems will be louder than modern, high-bypass ratio turbofans of comparable technology. People living near airports have the expectation of continuing the historical downward trend of aircraft noise.

NASA sets aggressive, strategic civil aircraft performance and environmental goals and develops ambitious technology roadmaps to guide its research efforts. Under NASA's Fundamental Aeronautics and Integrated Systems Research Programs, the Subsonic Fixed Wing and Environmentally Responsible Aviation Projects, respectively, have adopted community noise goals for the new, subsonic, single-aisle, civil aircraft expected to replace the current Boeing 737 and Airbus A320 families of airplanes. In NASA vernacular, these aircraft are designated as "N+1" vehicles since they will follow the current, in-service, "N" airplanes. NASA's N+1 community noise reduction goal calls for certification noise levels of 32 cumulative EPNdB under current FAA Part 36 Stage 4<sup>1</sup> and ICAO Chapter 4<sup>2</sup> noise limits.

A more challenging noise goal is set for the following generation of N+2 aircraft. This goal calls for a cumulative Stage 4 margin of 42 EPNdB. The additional 10 EPNdB margin is very ambitious, and it is thought by NASA not to be achievable by further reductions in engine and airframe noise sources alone. Instead, some sort of unconventional change in aircraft architecture, where propulsion noise sources are shielded from observers on the ground, is thought to be necessary to achieve the additional noise margin. The additional 10 EPNdB noise margin of the N+2 goal was set based on several preliminary studies of shielding benefits (e.g., Refs. 3, 4, 5).

Noise shielding (also referred to as barrier attenuation or insertion loss) is an acoustic diffraction phenomenon where acoustic waves are attenuated when propagated past an impermeable barrier placed between the noise source and an observer. Shielding is particularly efficient when the observer is located in the "shadow region" where the noise source is obscured. An obvious candidate for effective propulsion noise shielding is the proposed Blended Wing Body (BWB) aircraft. When turbofan engines are located above its large wing planform, a great deal of their fan and core noise would be shielded. Only jet noise – a distributed source generated downstream throughout the axial exhaust plume – would be difficult to effectively shield. Open rotor propulsion has been proposed for the BWB. Having little distributed jet noise,\* the relatively compact noise signature of an open rotor propulsor and its gas generator core may be more effectively shielded by a barrier than a turbofan.

Noise shielding is certainly not limited to BWB architectures, however. More conventional tube-and-wing aircraft may also provide some amount of noise shielding to open rotor propulsion systems. For example, one proposal for the Airbus A30X concept (Ref. 6, Fig. 1, left) has twin open rotor engines mounted to the aft fuselage, with the horizontal tail extending below and aft of counter-rotating propellers. The vertical twin tails, attached to the tailplane tips, are also likely to offer additional shielding benefit to lateral observers. Another notional concept is easyJet's ecoJet airplane (Ref. 7, Fig. 1, right). Its empennage is located below and forward of two open rotor propulsors. This "U-tail" empennage type of noise shielding is, most likely, less effective than the shielding provided by the BWB because of the relatively smaller blocking area.

Testing of various open rotor designs is underway in NASA Glenn's experimental facilities as part of an ongoing NASA-General Electric collaborative partnership.<sup>8</sup> Low-speed aerodynamic and acoustic tests were conducted in the Glenn 9- by 15-ft Low Speed Wind Tunnel, while (at this writing) high-speed aerodynamic testing is underway in the Glenn 8- by 6-ft tunnel. Noise data were collected during low-speed testing from an open rotor test article in a simulated flight environment with and without the presence of an acoustic barrier wall placed between the rotor and the microphone array. These shielded and unshielded acoustic data form the basis of this study.

\* Most of the core stream enthalpy is used to drive the power turbine, resulting in a low-energy exhaust.

The focus of this study is to predict the certification noise shielding system benefits that a U-tail empennage is likely to provide aircraft with twin open rotor engines mounted in the aft fuselage position. The additional cumulative margin of 10 EPNdB for NASA's N+2 noise goal was set largely via analytical means with relatively simple, first-order, low-fidelity tools. With the use of realistic, measured, acoustic shielding data, the results of this assessment will help in determining whether the additional 10 EPNdB of cumulative margin is reasonable.

The noise measurements are also compared to the simple, popular Maekawa empirical diffraction correlation often used at NASA to predict noise shielding (See Sections II.D and III.C.).

## II. Method of Analysis

In October, 2010, the acoustic data used in this study were collected from a counter-rotating, open rotor scale model in NASA Glenn's 9- by 15-ft Low Speed Wind Tunnel.<sup>9</sup> NASA's open rotor test rig was configured in these tests with General Electric's F31/A31 rotor blade set, with 12 forward rotor blades and 10 aft blades. The approximately one-fifth scale F31/A31 rotor set – often referred to as the “historical blade set” – dates to the Advanced Turboprop Project<sup>10,11</sup> of the 1980s. It is an unducted fan representative of an early 1990s technology level. The acoustic data collected from it is non-proprietary and may be published in the open literature. Additional details of the rotor design may be found in Ref. 12. Other, advanced-design, proprietary rotor sets incorporating innovative low-noise features and performance shaping of the airfoil stack derived through three-dimensional aerodynamic analysis have also been tested at NASA Glenn. Although the advanced rotors sets may be more representative of what may one day fly, the F31/A31 historical blade set serves as an approximate representation of a modern open rotor noise signature.

The tests at NASA Glenn were performed shortly before the joint NASA-Boeing propulsion-airframe aeroacoustic tests were completed at Boeing's Low-Speed Aeroacoustic Facility in November, 2010. The tests at Boeing used another historical open rotor test model: the F7/A7 (at approximately one-tenth scale), placed above a simulated BWB airframe and also at the rear of a simulated conventional fuselage. All of these tests are part of NASA's partnerships with U.S. industry to develop open rotor propulsion systems, but only the F31/A31 data collected at Glenn are used in this study.

### A. Data Collection

A long and a short acoustic barrier wall (first reported in 1997 in Ref. 13) were placed between the F31/A31 open rotor source and the linear microphone array as shown in Fig. 2. The impermeable barrier walls have been used in the facility to separate and mask noise sources radiating from targeted emission angles. For example, the long

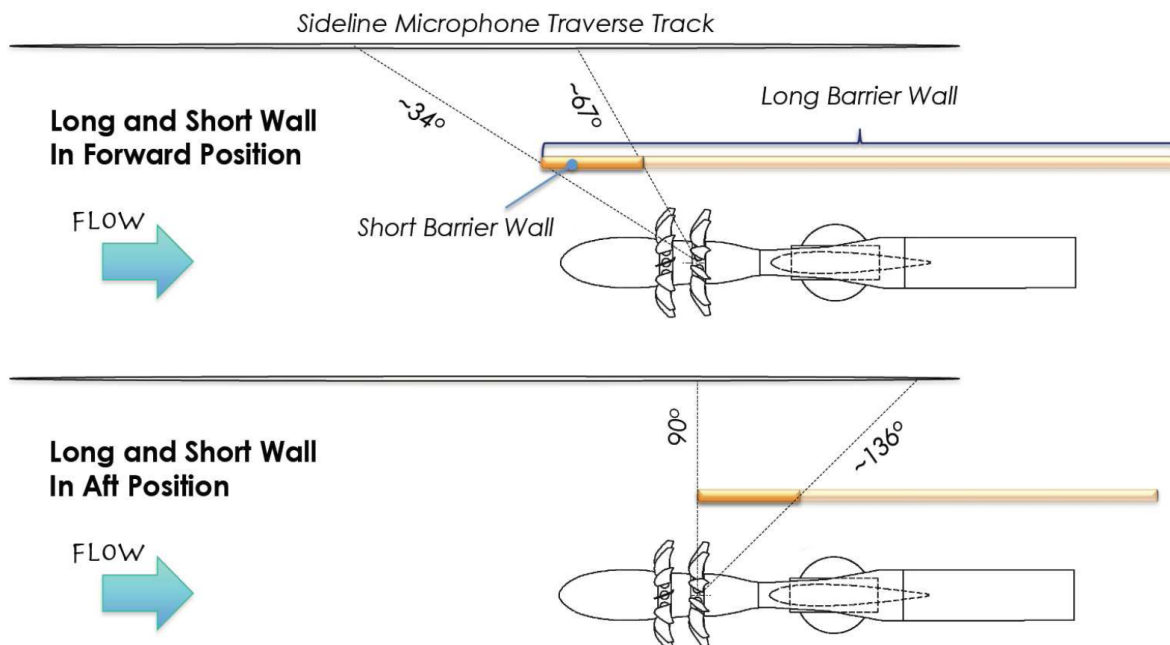


**Figure 2. F31/A31 open rotor test article and barrier wall positions in the NASA Glenn 9- by 15-ft Low Speed Wind Tunnel** (Diagram courtesy of Edmane Envira, NASA Glenn Research Center).

**Table 1. Locations of acoustic barrier wall relative to open rotor model.**

Wall Description	Wall Position	Wall Length	Location of leading edge of wall
Long	Forward	174.0 in.	40.375 in. upstream of center of aft rotor
Long	Aft	126.0 in.	Even with center of aft rotor
Short	Forward	28.625 in.	40.375 in. upstream of center of aft rotor
Short	Aft	28.625 in.	Even with center of aft rotor

wall has successfully been used to virtually remove the discharge noise of shrouded fan models by shielding it from the microphones so that forward-radiated fan noise may be more closely examined in isolation.

In the tests of the F31/A31 open rotor, the barrier wall was configured in four different ways as shown in Fig. 2. The zero reference of the geometric microphone yaw angle in the figure is directly upstream. The barrier in the “long wall” configuration approximates a theoretical semi-infinite shielding plane. Unfortunately, the long wall geometry is not a realistic representation of an open rotor in a BWB installation. The test article is located near the leading edge of the wall, and BWBs are not envisioned to use open rotors in a tractor implementation. Therefore, data with the long wall in place are not used in this assessment. The long wall data, however, are still of value to validate and verify analytical shielding prediction tools that predict diffraction in the presence of a semi-infinite wall.

The “short wall” configuration better represents the kind of empennage shielding expected of the aircraft illustrated in Fig. 1. The short barrier wall located in the aft position may represent the installation on the proposed open rotor version of the A30X, while the short wall in the forward position may represent the open rotor installation of the notional ecoJet. A photograph of the installation in the tunnel is shown in Fig. 3.

The barrier wall is 2.75 in. thick with an elliptical leading edge and a round trailing edge. The thickness of the wall and its rounded leading edge (in contrast to a sharp-edged, thin, flat plate, where diffraction behavior can be much different) contribute to the realism of the arrangement by roughly approximating an actual tailplane. The short barrier wall is 28.625 in. long and is located 26 in. from the centerline of the rotor model. The forward and aft rotor diameters are 25.7 in. and 24.8 in., respectively. As a point of reference, the short barrier wall is approximately twelve percent greater than one forward rotor diameter in length. The microphone traverse array is located 60 in. from the centerline of the rotor model. In the forward and aft wall positions, the wall leading edge is located 40.375 in. ahead of, and even with, the center of the aft rotor, respectively (See Table 1.).

Each tunnel “reading” consists of narrowband spectral density levels taken at 18 sideline microphone locations with frequencies ranging from zero to 100 kHz at frequency intervals of 12.2 Hz. Data with the open rotor model operating at corrected shaft speeds of 5550 rpm and 6300 rpm (85% and 96% of design speed) were collected. Both rotors always operated at identical shaft speeds. Tests were also made to estimate the facility’s background noise levels with no power supplied to the open rotor test article and with the blades windmilling.



**Figure 3. F31/A31 open rotor test article and “long” barrier wall in the NASA Glenn 9- by 15-ft Low Speed Wind Tunnel** (Photograph courtesy of David Stephens, NASA Glenn Research Center).

The spectral density levels are corrected by the facility's data acquisition software to lossless, freefield conditions using an atmospheric attenuation model. The spectral density levels are further corrected for spherical spreading from the microphone's constant sideline distance to a 1-foot constant radius arc.

Emission yaw angles ( $\theta_E$ ) are computed from the geometric sideline microphone array angles ( $\theta_G$ ) using the relation  $\theta_E = \theta_G - \sin^{-1}[M_{Tunnel} \sin \theta_G]$ , where the tunnel Mach number  $M_{Tunnel}$  in the experiments is 0.20. Data were also collected for  $M_{Tunnel} = 0.22$ , but they are not used in this assessment.

Insertion losses are calculated by Stephens in Ref. 9 by subtracting the measured spectral density levels of the open rotor tests conducted with and without the short barrier wall in place. These insertion losses are shown in Fig. 4 as a function of narrowband frequency and geometric yaw angle for the short barrier wall in the forward position. Note that positive values of insertion loss represent noise reductions perceived by the microphones. Also note that the data are plotted to frequencies of only 10 kHz. The insertion losses are shown for both tonal (left) and broadband (right) components. The shielding is the most effective in the deepest shadow zone of the wall (at about 51 degrees from the inlet), where the attenuation is 5 dB or greater. The barrier wall is partially effective (less than 5 dB) in the

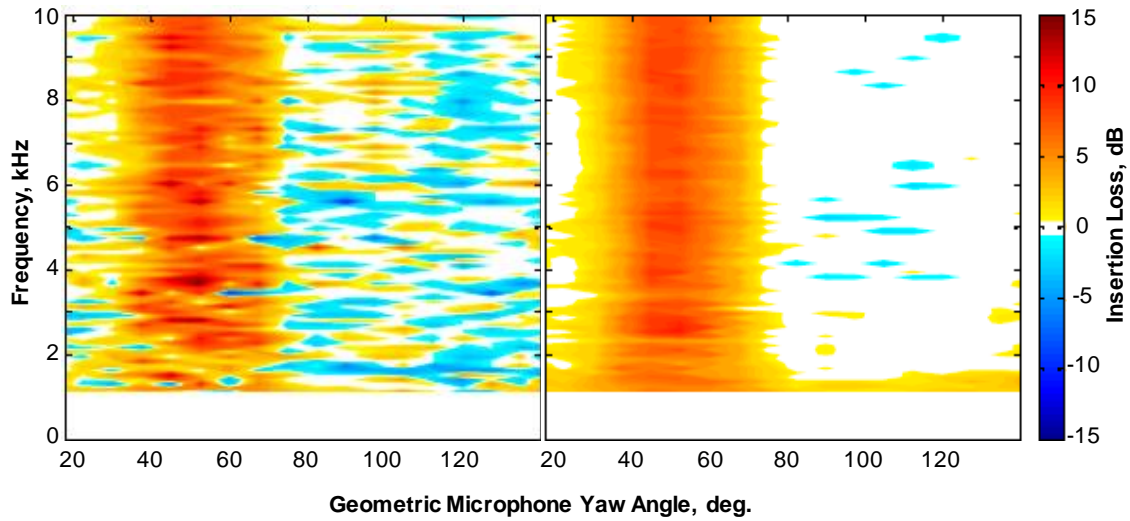


**Figure 4. Open rotor insertion loss at 6300 rpm with the short wall in the forward position; tones (left), and broadband (right) Plots courtesy of David Stephens, NASA Glenn Research Center (Ref. 9).**

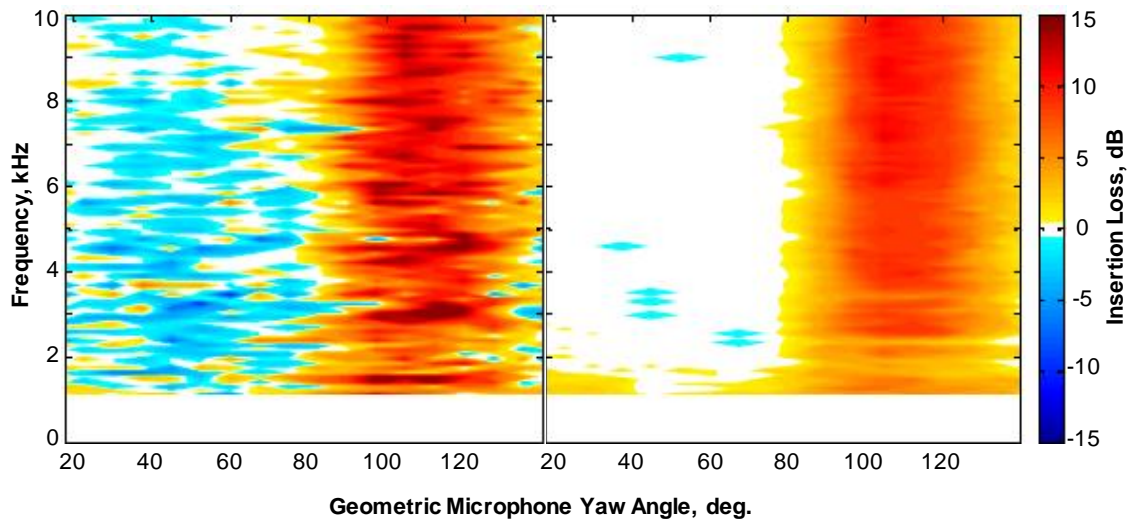


**Figure 5. Open rotor insertion loss at 6300 rpm with the short wall in the aft position; tones (left), and broadband (right) Plots courtesy of David Stephens, NASA Glenn Research Center (Ref. 9).**

transition zone, and it is not effective at all in the bright zone. There is, interestingly, some amplification of the noise – particularly of the rotor-rotor interaction tones – in the aft quadrant. In this area, the microphones perceive two constructively-interfering sources: from the source itself as well as from the noise diffracted at the edge of the wall. This noise amplification can be seen in the blue areas in Fig. 4. Similar insertion losses are shown in Fig. 5 for the short wall in the aft position. The corrected rotor shaft speeds in these tests are 6300 rpm.

## B. Data Manipulation

The measured, model-scale, narrowband data must be manipulated in several ways in order to properly compute certification noise shielding benefits for an actual, full-scale aircraft. The spectra have already been corrected by the facility's data acquisition software to freefield, lossless spectral density levels on a 1-foot arc. The spectra are modified further by applying the following corrections:

### 1. Removal of background facility noise

Noise measurements with the F31/A31 test article in an unpowered windmilling mode and with the tunnel in operation were conducted for each of the barrier wall configurations. The spectral density levels of the unpowered tests are subtracted from each noise spectrum of interest in the powered tests for frequencies less than 1000 Hz, where background facility noise is problematic and its removal is required. The spectral densities are then converted to sound pressure levels with a reference pressure of 20  $\mu$ Pa.

### 2. Conversion to static conditions

The sound pressure levels are corrected for convection effects to static conditions by adding an amplitude correction of  $10 \log_{10}[1 - M_{Tunnel} \cos \theta_E]^{SME}$ , where the source motion exponent (*SME*) is taken to be 4.0. No corrections are made to the frequency scale, since the microphones are “traveling with” the source at the speed of the tunnel Mach number, which in these cases is 0.20.

### 3. Conversion to flight conditions

The sound pressure levels are corrected to realistic takeoff and approach flight conditions by subtracting an amplitude correction of  $10 \log_{10}[1 - M_{Flight} \cos \theta_E]^{SME}$ . The flight Mach number,  $M_{Flight}$ , depends on airplane trajectory calculations for approach and departure, and are discussed in Sections II.C.1 and III.A below. The source motion exponent is again taken to be 4.0. A frequency shift of  $1 - [M_{Flight} - M_{Tunnel}] \cos \theta_E$  is applied to the frequency scale. An ambient source strength correction relative to international standard atmospheric (ISA) conditions of  $10 \log_{10}[(\rho/\rho_{ISA})^2 (c/c_{ISA})^4]$  is also made at this time, where  $\rho$  and  $c$  are the density and the speed of sound at the flight condition of interest, respectively. Standard acoustic day (ISA+18°F) conditions are used for this adjustment.

### 4. Conversion to full scale

The sound pressure levels are corrected from model scale to full scale using the linear scale factor (*LSF*) and the area scale factor (*ASF*). Amplitudes are adjusted by adding a correction of  $10 \log_{10}[ASF]$ , and frequencies are shifted to lower values by a factor of *LSF*. Based on current, parallel NASA open rotor system studies,<sup>14,15</sup> values for *LSF* and *ASF* are taken to be 5.27 and 27.8, respectively.

### 5. Conversion to 1/3<sup>rd</sup> octave band center frequencies

The frequency basis for FAA and ICAO aircraft noise certification is the traditional 1/3<sup>rd</sup> octave band center frequency spectrum, represented by 24 discrete sound pressure levels ranging from 50 Hz to 10,000 Hz. The acoustic energy contained in the intervals on either side of each center frequency (i.e., from  $2^{-1/8}$  times the center frequency to  $2^{1/8}$  times the center frequency) are summed to form each of the 24 standard 1/3<sup>rd</sup> octave band sound pressure levels.

Several of the above processes are illustrated in Fig. 6 using a sample spectrum taken from a microphone reading in the forward quadrant. A one-foot-arc, lossless, narrowband spectrum with facility noise removed is shown by the black line in Fig. 6 (left). This spectrum has an emission yaw angle of 24 degrees from the inlet, the tunnel Mach number is 0.20, and the F31/A31 open rotor test article is operating at a corrected shaft speed of 6300 rpm. The short barrier wall is not present. Although noise measurements are available up to 100 kHz, only lower-frequency data are plotted.

When flight condition scaling is applied (scaling to a flight Mach of 0.26 at 1000 ft is shown in the figure) the spectrum shifts to higher amplitudes and frequencies to the condition represented by the red line in the figure. Opposite shifting behavior occurs for spectra in the aft quadrant. Scaling from experimental tunnel conditions to appropriate, simulated flight conditions can result in changes of several decibels in the fore or aft quadrants and is thus an important processing step.

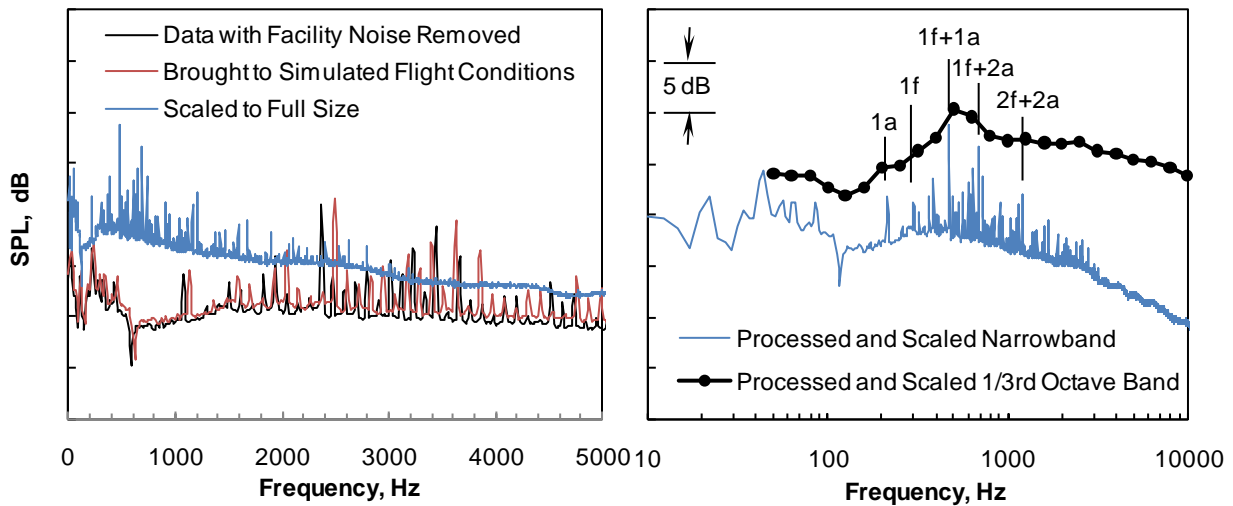


**Figure 6. Sample open rotor scale-model narrowband spectrum conversion to full size (left); and conversion from full-scale narrowband spectrum to standard 1/3<sup>rd</sup> octave band center frequencies (right).**

When the linear and area scale factors are applied, the spectrum shifts to much higher amplitudes and lower frequencies represented by the blue lines in both sides of the figure. At one-fifth scale, the inaudible sound pressure levels measured at frequencies of about 50 kHz are shifted to the audible, regulated range used to estimate noise certification levels.

The 1/3<sup>rd</sup> octave band sound pressure levels are computed as described above and are plotted in Fig. 6 (right). The fundamental blade passage frequency tones for the front and aft rotors are labeled “1f” and “1a” in the figure, respectively. Several higher-order rotor-rotor discrete interaction tones are also noted in the figure. Seldom do any of the interaction tones above the 2f+2a tone contribute significantly to the overall sound pressure level.

The reasoning behind the frequency “coarsening” from the narrowband to the 1/3<sup>rd</sup> octave band is that the resulting spectra become much easier to manipulate and store. Many of the rotor-rotor interaction tones lie within a single frequency interval, such that a single 1/3<sup>rd</sup> octave band sound pressure level may incorporate two (or more) tones, particularly at higher frequencies since the scale is logarithmic. In an open rotor aircraft noise certification test (or a simulation of one), the acoustic spectra observed by the microphone will fluctuate significantly as tones move from one frequency interval into another as the aircraft-observer geometry changes, and convective amplification and Doppler effects enter play. This will lead to irregular tone-weighted, perceived noise level (PNLT) time histories as the airplane traverses a path relative to its certification observers. This is an effect observed in large turboprops in the transport category as well, but it should be even more pronounced for an open rotor airplane with its much more complex tonal content.

The strategy of using unequal blade counts is apparent. With 12 blades on the front rotor and 10 blades on the aft rotor, and with both shafts turning at the same rate, the shaft tones are distributed more broadly throughout the spectrum. And when the narrowband spectra are “coarsened” to the 1/3<sup>rd</sup> octave band, much tone detail is lost and, in some cases, tones may not even be noticeable. This is a noise advantage not typically seen in conventional general aviation propellers, or even in civil aviation turboprop aircraft, where single-rotation propellers having more than six

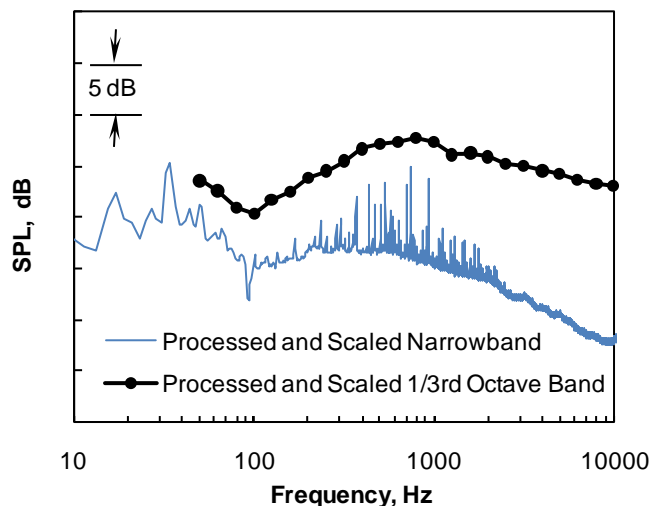


**Figure 7. Sample open rotor full-scale spectrum showing very little tonal penalty.**

blades are uncommon. Indeed, at some emission angles, scale factors and flight conditions, the tonal penalty may be insignificant. For example, for the case illustrated in Fig. 7, the tone penalty of the PNL metric is only 0.2 PNdB! The PNL metric is of particular importance since it is the basis of Part 36 noise certification.

### C. Computation of System Shielding Benefits

#### 1. Takeoff and Approach Trajectories

An analytical aircraft model with twin open rotor propulsion systems mounted on the aft fuselage is used in this assessment. Its general configuration is similar to the U-tail aircraft shown in Fig. 1. This notional airplane is used for the parallel NASA effort and is described in greater detail in Refs. 14 and 15. An airplane model with appropriate low-speed aerodynamics, weight, and propulsion performance data is necessary to model the takeoff and approach trajectories needed for aircraft certification predictions. The airplane is modeled using NASA's Flight Optimization System (FLOPS<sup>16</sup>) computer program. FLOPS computes detailed, low-speed takeoff and landing profiles using a built-in, time-stepping trajectory analysis module. Compliance with the airworthiness requirements described in Parts 36 and 25 of the Federal Aviation Regulations (Refs. 1 and 17, respectively) is observed.

#### 2. System Noise Prediction

The Aircraft Noise Prediction Program (ANOPP, Release Level 29)<sup>18,19</sup> is a systems-level code used in this study to compute certification noise for the open rotor airplanes. The center frequency basis for ANOPP is the 1/3<sup>rd</sup> octave band. The scaled 1/3<sup>rd</sup> octave band open rotor spectra described above are fed into ANOPP via its Acoustics Data Module (ACD<sup>20</sup>). ACD is an ANOPP utility that allows user-supplied spectra to be fed into a certification simulation in lieu of using ANOPP's own, built-in, source noise prediction modules.

Extreme care must be taken by users of ANOPP's ACD module, especially when attempting to model noise sources with tone content. As of ANOPP Level 29, the ACD module does not attempt to modify the user-input spectral content to account for convection effects as the airplane's airspeed and altitude vary throughout its trajectory. The onus therefore is on the user to supply proper spectra to ACD with a sufficient quantity of flight Mach numbers, and with the convection effects for each Mach number properly modeled and accounted for offline. Furthermore, the ACD module linearly interpolates for sound pressure level data between these flight Mach numbers, as well as across engine power setting, emission yaw angle, and emission roll angle. Quite often, a tone is improperly "washed out" by artifacts of interpolation. And perhaps even less obvious, a tone may be artificially diminished by interpolation error from simple convection effects. As Doppler shifts occur when the aircraft-observer geometry changes, a tone may move from one frequency interval into another and cause an interpolation error. Broadband noise is of course less prone to this effect. The solution to this problem is to eliminate interpolation error whenever possible by specifying data at the exact power settings required for the trajectory, and to minimize

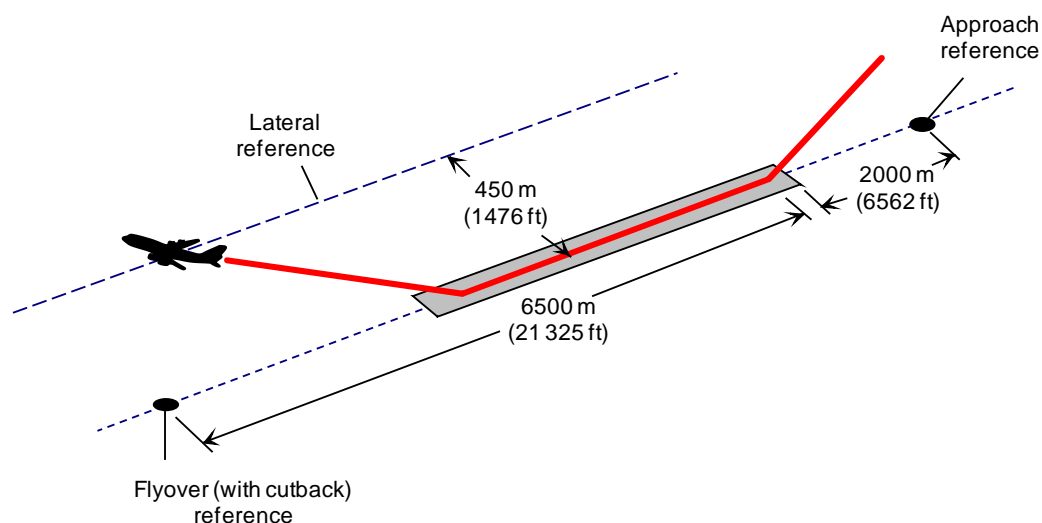


**Figure 8. Noise certification observer arrangement relative to hypothetical combined takeoff and landing aircraft trajectories.**

interpolation error by supplying data in sufficient quantity for the remainder of dependencies (i.e., flight Mach number and emission angles).

If tones under 800 Hz are propagated to an observer, Part 36 regulations permit them to be ignored – provided they can be shown to be unrelated to engine source noise – since they may be artifacts of ground reflections. Tones under 800 Hz, however, are very common for an open rotor propulsor (See, e.g., Fig. 6, right.). Thus, unlike most turbofan engine certification modeling, tones under 800 Hz are *not* ignored in this simulation and they *do* contribute to the PNLT.

The spectra are propagated to the three certification observers on the ground in accordance with the specifications for certification measurements. Noise propagation effects accounted for include spherical spreading, Doppler shift and convective amplification, atmospheric attenuation within a layered atmosphere, ground reflections based on data for grass-covered ground, and extra ground attenuation. More complex propagation phenomena such as scattering, weather effects, and terrain are not modeled. The airplane trajectory, computed by FLOPS as described above, is fed into the ANOPP simulation. Vector geometry analyses for the airplane relative to the three certification microphone measurement locations – shown in Fig. 8 – are performed within ANOPP as functions of source time. Note that in the interest of international rulemaking terminology harmonization, the former “sideline” certification location term has been deprecated in favor of “lateral,” as has “takeoff” to “flyover.” In any event, the propagated acoustic spectra are predicted at half-second intervals at each of the three certification locations on the ground. From these propagated spectra, ANOPP computes several noise metrics of interest as functions of observer time. The Effective Perceived Noise Level (EPNL) certification noise metric is computed from the noise-time history at each observer as prescribed in Ref. 1. In noise certification parlance, the cumulative, or algebraic, sum of the three certification EPNLs is often used to capture the range of operating conditions.

#### D. Comparison of Data to Maekawa Diffraction Model

The open rotor insertion loss data measured with the short barrier wall in place is compared to a simple empirical diffraction model based on asymptotic results of optical diffraction theory, originally proposed by Maekawa<sup>21</sup> and reproduced in many foundational acoustic textbooks (e.g., Ref. 22). The analytic treatment of diffraction effects in this manner is common in aeroacoustic applications. Being reliable, fast, and easy to implement, it has been coded into aircraft noise system prediction programs such as the General Aviation Synthesis Program<sup>23</sup> in 1982 and later into ANOPP.<sup>24</sup> Thus, any validation of the Maekawa model with respect to new, measured aeroacoustic data is a valuable undertaking.

Maekawa proposed the shadow zone barrier attenuation relation:

$$IL = 20 \log_{10} \left( \sqrt{2\pi|N_F|} / \tanh \sqrt{2\pi|N_F|} \right) + 5,$$

in dB, where  $N_F$  is the frequency-dependent Fresnel number ( $2f\Delta/c$ ), whose characteristic length  $\Delta$  is the difference between the shortest path around the barrier between the source and the observer and the source-observer distance directly through the barrier.

For observers in the bright zone ( $N_F < -0.192$ ), the attenuation is neglected, and for observers in the transition zone ( $-0.192 < N_F < 0$ ), it is appropriate to replace the hyperbolic tangent with the trigonometric tangent. Although the above relation is intended for use with semi-infinite barriers, Maekawa suggested that superposition may be used for barriers of finite length and width.

The Maekawa diffraction model is intended for insertion loss predictions of acoustically compact sources, where the geometry-dependent  $\Delta$  may be determined using distances relative to a radiating point source. When the Maekawa relation is used in this investigation, the entire open rotor test article is assumed to be a compact point source radiating from the center of the aft rotor. The open rotor model, however, is not at all compact. Very efficient

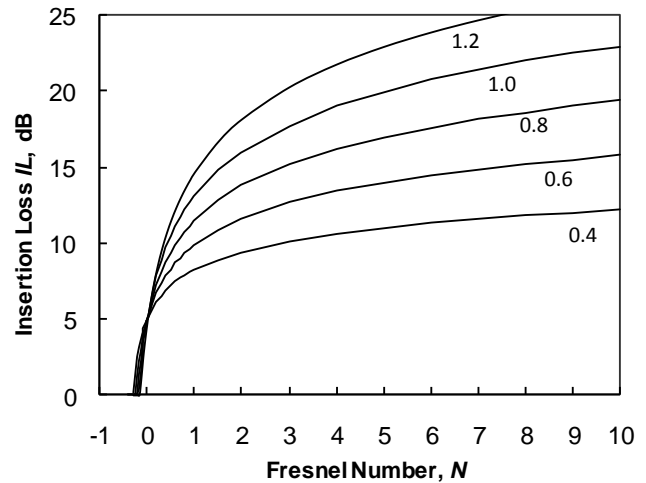


Figure 9. Modified Maekawa insertion loss relation showing influence of calibration constant  $a_1$ .

noise generation occurs nearer the rotor tips, at more than 12 inches from the rotor axis. Using the Maekawa relation in this way pushes it beyond its intended capability.

A modified relation is proposed here:

$$IL = 20 a_1 \log_{10} \left( \sqrt{2\pi |N_F|} / \tanh \sqrt{2\pi |N_F|} \right) + 5 + a_2,$$

where  $a_1$  and  $a_2$  are proposed new calibration constants intended to improve the prediction with respect to the open rotor data measured in this experiment. The influence of  $a_1$  on  $IL$  is shown in Fig. 9. It has the effect of reducing the magnitude of  $IL$  in the shadow zone while having a lesser impact in the transition zone.  $a_2$ , of course, simply shifts the entire relation. In the figure,  $a_2$  is zero. A value of unity for  $a_1$  yields Maekawa's original relation.

### III. Results and Discussion

#### A. Trajectory Results

Takeoff and approach trajectories and throttle settings must be modeled properly to correctly compute certification noise. An open rotor propulsor's thrust characteristics differ from the performance of turbofans, and thus a trajectory calculation is necessary to capture these effects. This is often in contrast to many other certification noise estimates made during the conceptual phase of aircraft design, where fixed trajectories and throttle settings are often assumed based on previously-collected data from other representative aircraft.

Trajectory data computed for the open rotor airplane for altitude above field elevation (AFE), airspeed, and

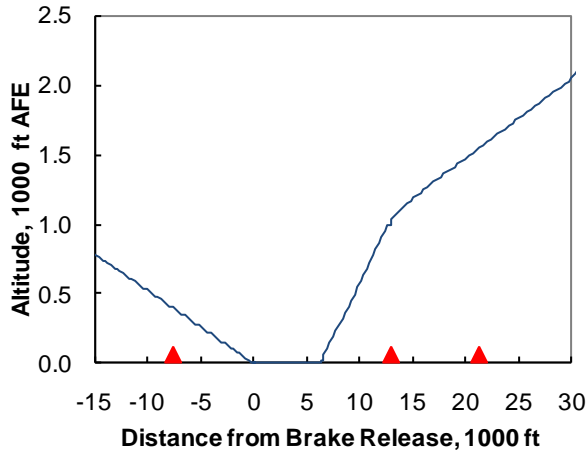


Figure 10. Open rotor airplane altitude.

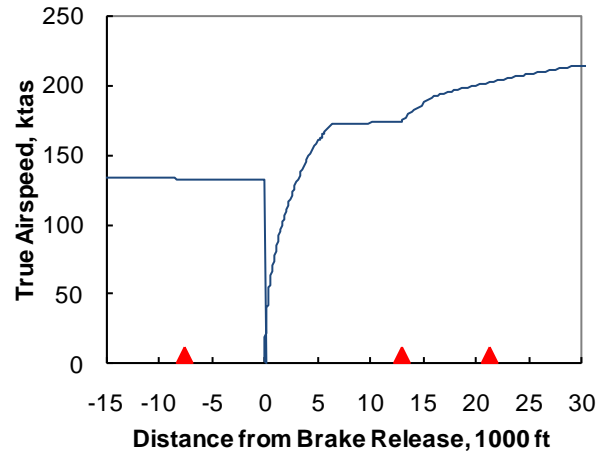


Figure 11. Open rotor airplane airspeed.

throttle setting are shown in Fig. 10, Fig. 11, and Fig. 12, respectively. The trajectory shown is presented as an operation with both takeoff and landing data shown simultaneously. For presentation purposes, the touchdown point on landing is coincident with the point of brake release on takeoff. Calculations are made for a sea level runway at standard acoustic day (ISA+18°F) conditions. The triangular markers on each plot denote the three noise certification measurement locations.

The approach microphone markers are shown in the figures at 6562 ft (2000 m) behind the runway threshold (i.e., behind the location of the 50 ft landing obstacle), and 7518 ft from the touchdown point on the runway centerline. The lateral microphone markers are shown in the figures at 13,000 ft from brake release, on a lateral sideline displacement distance of 1476 ft

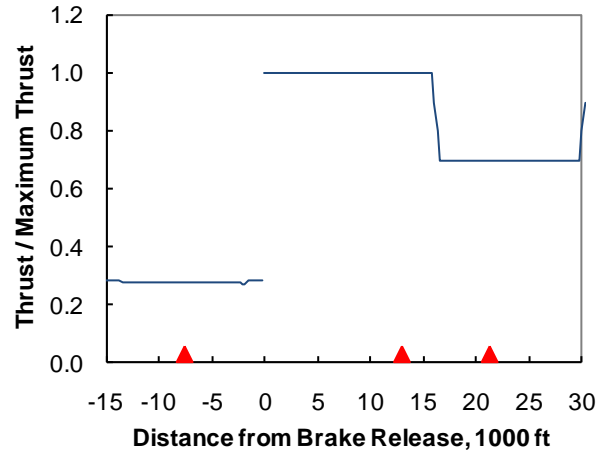


Figure 12. Open rotor airplane throttle setting.

(450 m) from the runway centerline. The 13,000 ft location corresponds to the distance from brake release where the airplane has reached 984 ft (300 m) AFE, as permitted – when approved – by regulation B36.3.a.1 (Ref. 1). A check of other lateral locations less than and greater than 13,000 ft from brake release confirms that peak lateral EPNL does in fact occur approximately at the 13,000 ft location. The flyover microphone markers are shown in the figures at 21,325 ft (6500 m) from brake release on the runway centerline. A noise abatement throttle cutback is used. The engine climb thrust at this point is reduced to the minimum level permitted by regulation (i.e., Ref. 1 requires a minimum climb gradient of four percent with both engines operating, or level flight with one engine inoperative.). The throttle cutback takes place between 16,000 ft and 17,000 ft from brake release. Note the power cutback takes place at approximately 1300 ft AFE. This is above the minimum altitude permitted (i.e., 984 ft, or 300 m AFE for a twin-engine airplane), in an attempt to gain additional altitude and to minimize the noise at the flyover observer.

The computed trajectories and throttle settings are used to guide the open rotor data scaling process described in Section II.B.3. For the barrier wall tests conducted in October, 2010, the F31/A31 test article was operated at only two shaft speeds. Based on guidance from the open rotor propulsion system model analyzed by Hendricks (Ref. 14), the acoustic data collected at the corrected shaft speed of 5550 rpm is used to predict the approach observer noise, while the data collected at the corrected shaft speed of 6300 rpm is used for the both lateral and flyover noise predictions. These shaft speeds are equivalent to 1050 rpm and 1200 rpm after scaling to full size with a linear scale factor of 5.27, respectively.

## B. Certification Noise Results

The variation of PNLT with emission yaw angle is shown in Fig. 13 for the unshielded source (solid black lines) along with PNLTs of the source shielded by the short wall in the forward (top) and aft (bottom) positions. The lossless, freefield data are shown on a constant, 1-foot arc. They have been scaled using values for *LSF* and *ASF* of 5.27 and 27.8, respectively, using a flight Mach number of 0.30. The test article corrected shaft speed is 6300 rpm, with the effects of scaling simulating a speed of 1200 rpm. The shielding benefits of the short wall are apparent: insertion losses as high as 8.8 PNdB are present with the wall in either position.

The PNLT scale is not shown in the figure since only the differences in PNLT (and EPNL) are important in this study of noise shielding. Emphasis is not placed on the absolute predicted levels of the EPNLs, but rather on the differences between them. The F31/A31 open rotor (an early 1990s design) is also not quite representative of a modern open rotor design that may one day fly. Advanced open rotor propulsors will be designed using 3D aerodynamic analytical tools and will employ advanced, low-noise features: some of which have been made public and others that are still company-proprietary. Noise mitigation strategies that have been made public<sup>25</sup> include aeroacoustic blade shaping, blade pitch angle and rotational speed optimization, increased blade counts, low disk loading, rotor-rotor spacing and pylon-rotor spacing optimization, aft rotor clipping, and pylon wake reduction. Moreover, the data collected with the barrier wall in place did not have a simulated pylon or fuselage installed, nor was there any variation in angle of attack. \* The aerodynamic installation is known to have a significant effect on open rotor noise (See, e.g., Ref. 26.).

The next step in assessing the system-level benefit of the insertion loss is to compute the certification EPNLs. The overall noise benefit is not readily apparent from Fig. 13 alone, since trajectory effects come into play. The PNLT-time noise history naturally rises and falls as the source first approaches – and then recedes from – a ground-

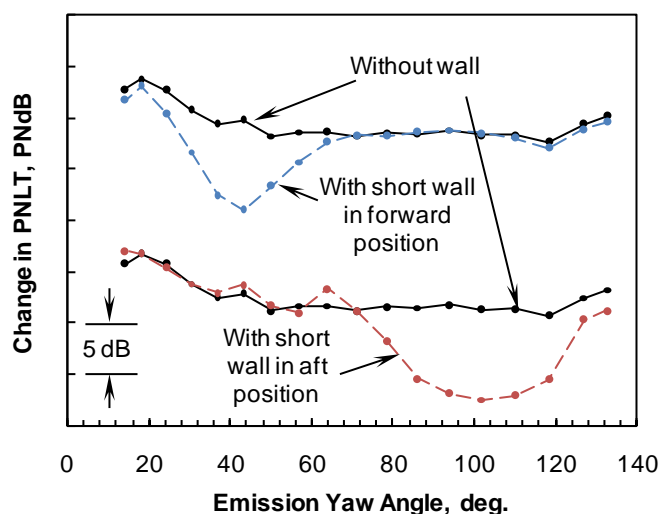


**Figure 13. Variation of PNLT with emission yaw angle, with and without barrier walls** (*Lossless data on 1-ft arc, scaled to full size and to flight Mach 0.30. Note vertical offset shift for clarity.*).

\* These influence of these effects were measured in other tests at the NASA Glenn facility, but not in the tests made with the barrier wall.

based observer. The source's directivity pattern and source-motion convection effects also play important roles in this noise system problem.

The benefit of the insertion loss may be squandered if the peak PNLT perceived by an observer occurs at an angle where there is no shielding benefit. Correct placement of the propulsors relative to the U-tail is important if any system noise shielding benefit is expected.

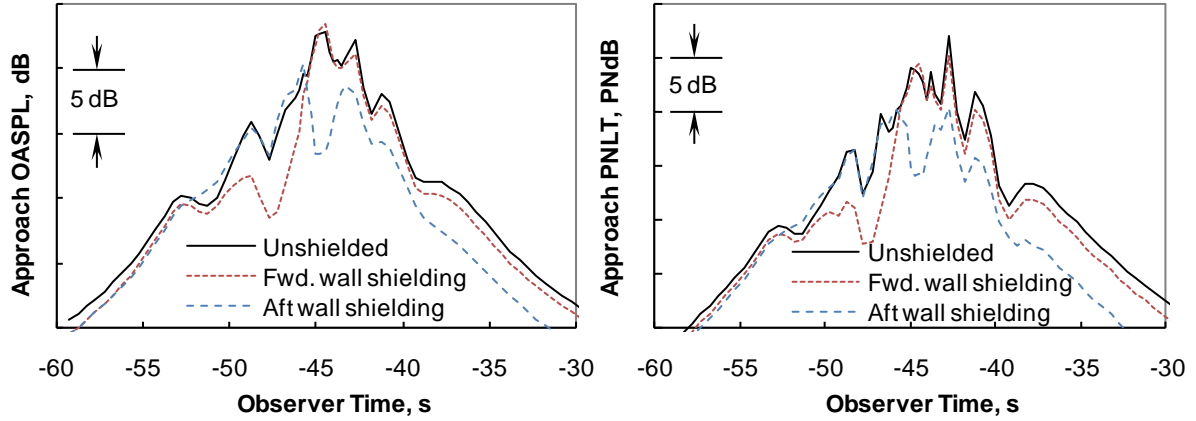


Figure 14. Approach observer OASPL noise-time histories (left), and PNLT noise-time histories (right).

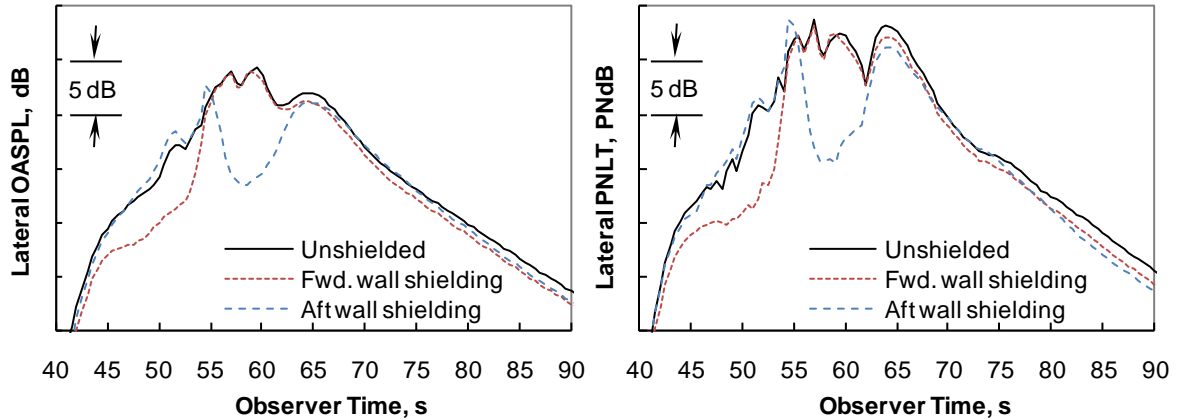


Figure 15. Lateral observer OASPL noise-time histories (left), and PNLT noise-time histories (right).

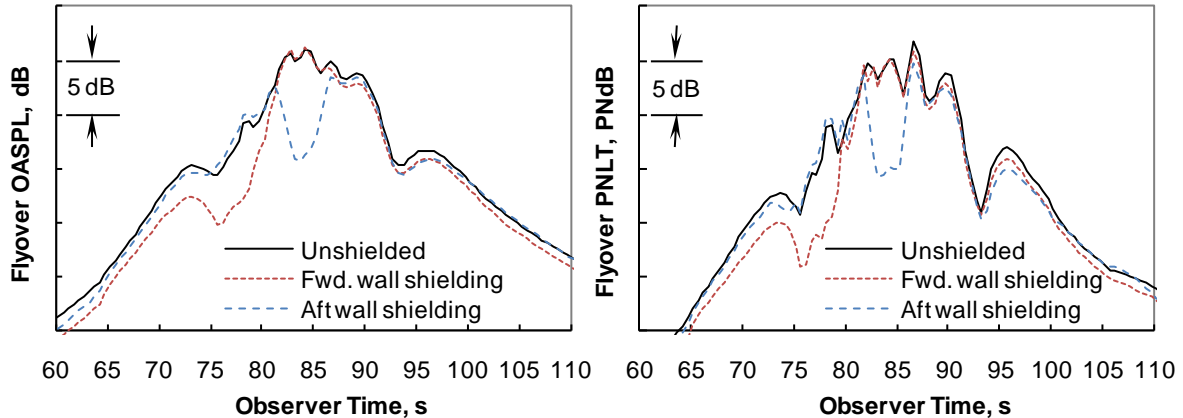


Figure 16. Flyover observer OASPL noise-time histories (left), and PNLT noise-time histories (right).

The scaled acoustic data are used to generate spectra at half-second time intervals along the trajectory. The spectra are propagated to each observer, and the overall sound pressure level (OASPL) and PNLT noise-time histories are computed and plotted in Fig. 14, Fig. 15, and Fig. 16 for the approach, lateral, and flyover observers, respectively. Observer time relative to the point of brake release (or touchdown) is used as the independent parameter in each figure. The OASPL metric is shown on the left in each figure because of its simplicity and its ability to clearly show the relatively smooth rise and fall of each noise source over time. The PNLT metric – shown on the right in each figure – has qualities that capture level, frequency weighting, and tone annoyance penalties. Its time histories are therefore much more irregular than the OASPL histories: as the airplane approaches and recedes, Doppler and convective amplification effects influence the PNLT metric's frequency-weighting and tone penalties. Only the PNLT-time histories within an integration region of 10 PNdB from the maximum PNLT are used to compute EPNLs.

From the appearance of the figures, the short barrier wall in the aft position seems to be nearly ideally placed: the maximum insertion loss approximately coincides with the peak PNLT of the unshielded source. The EPNL shielding benefits of the barrier wall in the forward and aft positions are shown in Table 2. The maximum shielding benefit is approximately 8 cumulative EPNdB.

**Table 2: EPNL benefit due to shielding for each observer (EPNdB)**

Wall position	Lateral	Flyover	Approach	Cumulative
Forward	-0.9	-0.8	-1.2	-2.9
Aft	-2.7	-2.2	-3.4	-8.3

Although 8 EPNdB falls short of the 10 EPNdB that is required for the NASA goal, there is some reason to believe that the shielding benefits calculated here may be somewhat conservative. Certainly a blended wing body airplane, with far more shielding surface area than a conventional airframe configuration, is likely to provide a greater shielding benefit. Forward-radiated propulsor noise may be virtually eliminated on such an architecture. But even for the tube-and-wing airplane assumed here, where the shielding surface is small relative to a BWB planform, the shielding benefit may be underestimated. For a lateral observer, there would undoubtedly be additional shielding of one of the open rotor propulsors by the rear fuselage that is not accounted for in this assessment.

On the other hand, there is also reason to believe that the insertion losses measured in the Glenn facility are greater than what would be observed in actual flight. In an in-flight application, ground observers would be located much further away from the source and the barrier than the microphones are in the Glenn facility. In the experiment, the microphone array is only 60 inches away from the centerline of the open rotor rig, and just 31 inches away from the acoustic barrier wall. This geometry results in Fresnel numbers that are higher than they would be in an actual flight test. In an airplane flyover condition, the source-to-observer distances are very large relative to the source-to-shield distance. In a flyover, the characteristic lengths of the Fresnel number ( $\Delta$ ) would approach their asymptotic limits. This effect is shown graphically in Fig. 17. In the figure, the Fresnel number (at 1000 Hz) is computed for varying source-to-microphone distances for an emission yaw angle of 102 degrees with the short barrier wall located in the aft position. A figure like this could be drawn for any geometry, but this emission angle is chosen in particular because it lies in the deepest part of the shadow zone. The barrier wall and open rotor test article geometry remains fixed. The Fresnel number for the geometry in the facility is 1.7 (marked by the symbol in the figure), while its asymptotic limit is about 1.0. For any given observer location, the Fresnel numbers of the

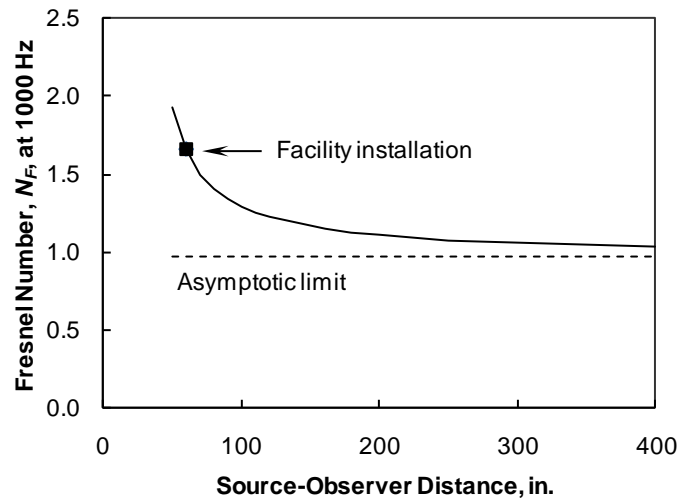


**Figure 17. Variation of leading-edge Fresnel number with source-to-observer distance (Frequency 1000 Hz, emission yaw angle 102 deg., barrier wall in aft position).**

experiment are higher than they would be in an actual flight test. The actual noise shielding benefit in flight therefore may be expected to be less than the benefit indicated by the experimental data.

Other sources of noise would also exist. In addition to the open rotor propulsor noise, core noise radiating from the gas generator, turbulent flow noise sources radiating from parts of the airframe, and even some jet noise from the exhaust will combine to form the overall noise signature of the airplane. Except for the gas generator core noise, the U-tail would provide little or no shielding, and the overall shielding benefit predicted here would shrink.

Given these issues, an uncertainty analysis of the EPNL calculations presented here is difficult to perform with the data available here alone. It should be noted, however, that noise shielding data collected within the confines of *any* relatively small facility would be prone to the same limitations. It is therefore advisable, perhaps, that any experimental shielding data collected in a facility be used to validate and verify more accurate analytical acoustic diffraction tools, which in turn could be used to more accurately predict the certification noise benefits of shielding.

### C. Comparison with Maekawa Diffraction Model

The insertion losses are shown in Fig. 18 for the short barrier wall in the forward position. The measured insertion loss (indicated by the blue line) is determined by subtracting the spectra recorded with the barrier wall in place from the spectra recorded without the wall. No scaling of the data is performed. In other words, the sound spectra are left unadjusted for size and convection effects, with  $LSF = ASF = 1$  and  $M_{Tunnel} = 0.20$ . The data are presented on a constant 1-foot arc. All insertion losses are summed to OASPLs so that their variations with emission angle can be more easily shown in the figure. The maximum OASPL reduction (8 dB) occurs in the shadow zone, at an emission yaw angle of 43 degrees.

The Maekawa diffraction model described in Section II.D is used to predict the insertion loss. For this purpose, the open rotor test article is assumed to be an acoustically-radiating point source. The source location used to compute the characteristic lengths ( $\Delta$ ) is taken to be at the center of the aft rotor. The loss predicted by the unmodified, original Maekawa relation – that is, with the calibration constant  $a_1$  set to unity and  $a_2$  set to zero – is indicated by the red line in the figure.

The Maekawa relation appears to overpredict the maximum insertion loss by about 13 dB. The method, however, is being used beyond its original scope. With forward and aft rotor diameters of 25.7 in. and 24.8 in., respectively, and with efficient noise generation occurring near the rotor tips, the open rotor model is certainly not a compact source. Computing Fresnel numbers in this manner introduces error.

The method can make an improved prediction by altering the calibration constants  $a_1$  and  $a_2$  from their neutral values of unity and zero, respectively. Setting  $a_1 = 0.3$  with  $a_2 = 0$ , or setting  $a_2 = -14$  with  $a_1 = 1.0$  provides a better fit of the data. The predicted insertion loss using  $a_1 = 0.3$  and  $a_2 = 0$  is indicated by the green line in the figure. These calibration values match the shielded data equally well when the wall is in the aft position.

From an ANOPP user's perspective, however, it is not possible to implement alternative values of  $a_1$  or  $a_2$ ; at least via the ordinary use of the WING module. The Maekawa method, as coded into WING, does not allow Maekawa's relation to be customized via user input. Furthermore, the output of the WING module (a data table that is also named "WING") is not defined to the database manager, so that any other modules that are designed to alter data tables (e.g., the General Suppression Module<sup>27</sup>), cannot be used.

Possibly the only way to alter the values in the WING data table would be to unload the member data into an external file, manipulate the data by means of some offline analysis, and load the revised member data back into the user's simulation. This approach would be very tedious. Modifying the source code with new features may be the only practical option.

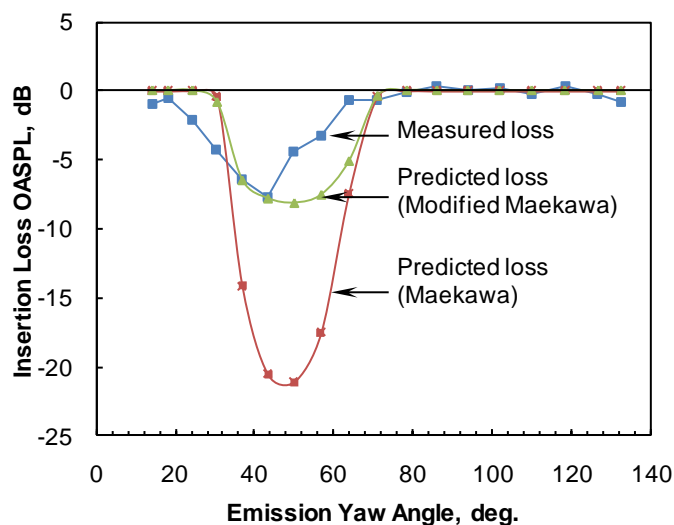


**Figure 18. Measured and predicted insertion losses with the short barrier wall in the forward position (Data on 1-ft arc, tunnel conditions, no size scaling).**

Another alternative is to wait for a higher-order diffraction method to be implemented into ANOPP. The Maggi-Rubinowicz formulation of Kirchhoff's diffraction theory<sup>28</sup> is anticipated to be programmed into a release of ANOPP later in 2011.

#### IV. Conclusions

The first phase of NASA's noise reduction goal calls for aircraft with cumulative Stage 4 margins of 32 EPNdB. The second phase requires an additional margin of 10 EPNdB. The second phase is thought by NASA not to be achievable by reductions in engine and airframe noise sources alone. A change in aircraft architecture, where propulsion noise sources are shielded from observers on the ground, is thought to be necessary to achieve the additional noise margin.

This study focuses on predicting the noise certification benefits of a notional open rotor aircraft with empennage shielding a portion of the rotor noise. Twin, aft-fuselage-mounted, open rotor propulsors are partially shielded by a U-tail structure. The basis of the prediction are noise measurements of an open rotor test article collected with and without an acoustic barrier wall that simulates the U-tail. The chord length of the simulated U-tail is twelve percent greater than the forward rotor diameter. Two tail positions are analyzed. When the tail is located in the aft position, the cumulative system noise benefit is predicted to be 8 EPNdB. The tail in the aft position appears to be ideally located to reduce noise perceived by noise certification ground observers. With the tail in the forward position, the cumulative noise reduction is predicted to be only 3 EPNdB.

The predicted 8 EPNdB margin is encouraging for the tube-and-wing airplane assumed here. A blended wing body airplane, with far more shielding surface area than a conventional airframe configuration, is likely to provide an even greater shielding benefit. Forward-radiated propulsor noise may virtually be eliminated on such an architecture.

However encouraging these results may be, the acoustic data used in this analysis may not be ideally suited to make a systems noise prediction. The measurements were collected within the confines of a relatively small facility, where the insertion loss benefits are likely to be exaggerated relative to those that would be experienced during an actual airplane flyover. However, the experimental shielding data collected in this study could be used to help validate and verify more accurate analytical acoustic diffraction tools. These, in turn, could be used to more accurately predict the certification noise benefits of shielding.

#### Acknowledgments

Thanks go to David Stephens, David Elliott, and Dale Van Zante of NASA's Environmentally Responsible Aviation Project for collecting and providing the open rotor acoustic data used in this study. Thanks also go to Edmane Envia and the Subsonic Fixed Wing Project for providing the opportunity and resources to study the data.

#### References

- <sup>1</sup>U.S. Code of Federal Regulations, Title 14, Chapter I, Part 36, *Noise standards: Aircraft Type and Airworthiness Certification*.
- <sup>2</sup>*International Standards and Recommended Practices – Environmental Protection, Annex 16 to the Convention on International Civil Aviation, Volume I: Aircraft Noise*, 3<sup>rd</sup> Edition, International Civil Aviation Organization (ICAO), Montreal, Canada, July 2008.
- <sup>3</sup>Berton, J.J.: "Noise Reduction Potential of Large, Over-the-Wing Mounted, Advanced Turbofan Engines," ISABE XIV Paper 99-7254, 1999, and NASA/TM-2000-210025, 2000.
- <sup>4</sup>Hill, Geoffrey, A.: *Aerodynamic and Acoustic Investigations of an Advanced Over-the-Wing Nacelle Transport Aircraft Configuration*, Master's Thesis, Old Dominion University, Norfolk, VA, 2007.
- <sup>5</sup>Thomas, R.: "Subsonic Fixed Wing Project N+2 Noise Goal Summary," presentation at the NASA Acoustics Technical Working Group, Cleveland, OH, December 4-5, 2007.
- <sup>6</sup>Airbus: *Global Market Forecast 2009-2028*, URL: <http://www.airbus.com/en/corporate/gmf2009> [cited 11/2/2010].
- <sup>7</sup>easyJet, Ltd., press release: *The "easyJet ecoJet" to cut CO<sub>2</sub> emissions by 50% by 2015*, June, 2007, URL: [http://www.easyjet.com/en/news/easyjet\\_ecojet.html](http://www.easyjet.com/en/news/easyjet_ecojet.html) [cited 11/2/2010].
- <sup>8</sup>NASA Press Release (Vol. 2, Issue 3, March 30, 2009): *GE and NASA Partner on Open Rotor Engine Testing*, URL: [http://www.nasa.gov/offices/oce/appel/ask-academy/issues/volume2/AA\\_2-3\\_F\\_ge\\_rotor.html](http://www.nasa.gov/offices/oce/appel/ask-academy/issues/volume2/AA_2-3_F_ge_rotor.html) [cited 4/8/2011].
- <sup>9</sup>Stephens, D.; and Envia, E.: "Acoustic Shielding for a Model Scale Counter-rotation Open Rotor," 17<sup>th</sup> AIAA/CEAS Aeroacoustics Conference (32<sup>nd</sup> AIAA Aeroacoustics Conference), AIAA paper to be published, June, 2011.
- <sup>10</sup>Hager, R.; and Vrabel, D.: "Advanced Turboprop Project," NASA SP-495, April, 1988.
- <sup>11</sup>Hoff, G., et al.: "Experimental Performance and Acoustic Investigation of Modern, Counterrotating Blade Concepts," NASA CR-185158, Jan., 1990.

- <sup>12</sup>Delaney, B.R.; Balan, C.; West, H.; Humenik, F.M.; and Craig, G.: "A Model Propulsion Simulator for Evaluating Counter Rotating Blade Characteristics," SAE Paper 861715, Aerospace Technology Conference and Exposition, Long Beach, CA, Oct. 13-16, 1986.
- <sup>13</sup>Woodward, R.; Elliott, D.; Hughes, C.; and Berton, J.: "Benefits of Swept and Leaned Stators for Fan Noise Reduction," November/December 2001 Journal of Aircraft; also NASA TM-208661, 1998; and AIAA-99-0479, 1998.
- <sup>14</sup>Hendricks, E.S.: "Development of an Open Rotor Cycle Model in NPSS using a Multi-Design Point Approach," Proceedings of ASME Turbo Expo, GT2011-46694, to be published, June 2011.
- <sup>15</sup>Guynn, M.D.: "Initial Assessment of Open Rotor Propulsion Applied to an Advanced Single Aisle Aircraft," 11<sup>th</sup> AIAA Aviation Technology, Integration, and Operations (ATIO) Conference, AIAA paper to be published, September 2011.
- <sup>16</sup>McCullers, L.A.: "Aircraft Configuration Optimization Including Optimized Flight Profiles," *Proceedings of the Symposium on Recent Experiences in Multidisciplinary Analysis and Optimization*, NASA CP 2327, April 1984.
- <sup>17</sup>U.S. Code of Federal Regulations, Title 14, Chapter I, Part 25. *Airworthiness Standards: Transport Category Airplanes*.
- <sup>18</sup>Gillian, R.E.: "Aircraft Noise Prediction Program User's Manual," NASA TM-84486, 1983.
- <sup>19</sup>Zorumski, W.E.: "Aircraft Noise Prediction Program Theoretical Manual," NASA TM-83199, 1981, Parts 1 and 2 (Currently maintained at NASA Langley Research Center by the ANOPP team in electronic format and provided upon request; Latest revision: April, 2011).
- <sup>20</sup>Rawls, J.: "ACD Module," *ANOPP Theoretical Manual*, ver. 29, NASA Langley Research Center, Hampton, VA, 2011.
- <sup>21</sup>Maekawa, Z.: "Noise Reduction By Screens," *Memoirs of the Faculty of Engineering*, Vol. 12, Kobe University, Kobe, Japan, 1966, pp. 472-479.
- <sup>22</sup>Beranek, L.L.: *Noise and Vibration Control*, McGraw-Hill, New York, 1971, pp. 174-180.
- <sup>23</sup>Mitchell, J.; Barton, C.; Kisner, L.; and Lyon, C.: "Computer Program to Predict Noise Levels of General Aviation Aircraft: User's Guide," NASA CR-168050, 1982.
- <sup>24</sup>Weir, D.: "WING Module," *ANOPP Theoretical Manual*, ver. 29, NASA Langley Research Center, Hampton, VA, 2011.
- <sup>25</sup>Majjigi, M.; and Wojno, J.: "Previous Open Rotor Noise Experience at GE," General Electric Presentation, X-Noise Open Rotor Technology Seminar, Lausanne, Switzerland; March 18, 2011.
- <sup>26</sup>Lempereur, P.: "Advances in Knowledge of Noise Impact of Installation and Aircraft Configuration," Airbus Presentation, X-Noise Open Rotor Technology Seminar, Lausanne, Switzerland; March 18, 2011.
- <sup>27</sup>Zorumski, W.E.: "GENSUP Module," *ANOPP Theoretical Manual*, ver. 29, NASA Langley Research Center, Hampton, VA, 2011.
- <sup>28</sup>Lummer, M.: "Maggi-Rubinowicz Diffraction Correction for Ray-Tracing Calculations of Engine Noise Shielding," 14<sup>th</sup> AIAA/CEAS Aeroacoustics Conference (29<sup>th</sup> AIAA Aeroacoustics Conference), AIAA paper 2008-3050, 2008.